Ultrasound localization microscopy of the human kidney allograft on a clinical ultrasound scanner

Sylvain Bodard, Louise Denis, Vincent Hingot, Arthur Chavignon, Olivier Hélénon, Dany Anglicheau, Olivier Couture, Jean-Michel Correas

Ultrasound Localization Microscopy of the human kidney allograft on a clinical ultrasound scanner

Authors: Sylvain Bodard MD[1,2,3*], Louise Denis MS[2*], Vincent Hingot PhD[2], Arthur Chavignon PhD[2], Olivier Hélénon MD[1,3], Dany Anglicheau MD PhD[3,4], Olivier Couture PhD[2], Jean-Michel Correas MD PhD [1,2,3]

** These authors contributed equally to this work*
1 AP-HP, Hôpital Necker Enfants Malades, Service d'Imagerie Adulte, F-75015, Paris, France
2 Sorbonne Université, CNRS, INSERM Laboratoire d'Imagerie Biomédicale, Paris, France
3 Université de Paris Cité, Paris, France
4 AP-HP, Hôpital Necker Enfants Malades, Service de néphrologie-transplantation rénale adulte, F-75015, Paris, France

Corresponding authors: sylvainbod@hotmail.com

Source of support: European Research Council

Running Headline: Non-invasive and quantitative imaging tool on the human kidney graft

Word Count:
- Abstract: 188
- Introduction: 453
- Methods: 108
- Results: 295
- Discussion: 579

ABSTRACT

Chronic kidney disease is a major medical problem, causing more than a million deaths each year in the world. Peripheral renal microvascular damage is found in most chronic kidney diseases, yet noninvasive and quantitative diagnostic tools are still lacking. Ultrasound Localization Microscopy (ULM) can assess tissue microvasculature with unprecedented resolution.

In this work, we studied the feasibility of ULM in human kidney allografts with a standard low frame rate ultrasound scanner. The acquisition parameters were derived from Contrast-Enhanced Ultrasound (CEUS) examinations by increasing the duration of the recorded clip at the same plane. ULM images were compared with Color Doppler, Advanced Dynamic Flow (ADF), and Superb Microvascular Imaging (SMI) with a contrast agent. Despite some additional limitations due to movement and saturation artifacts, ULM identified vessels 2 to 4 times thinner compared with Doppler modes; i.e. the mean ULM smallest analyzable vessel cross section is 0.3 ± 0.2 mm in 7 patients. Additionally, ULM was able to provide quantitative information on blood velocities in the cortex area.

In this proof-of-concept study, ULM was shown to be a promising imaging technique for the qualitative and quantitative assessment of microvessels.

Keywords: Ultrasound Localization Microscopy, super resolution, renal transplantation, renal ultrasound imaging

INTRODUCTION

Chronic kidney disease (CKD) causes more than one million deaths worldwide each year [1]. This pathology is affected by acute kidney injury, age, and comorbid conditions [2,3] and is associated with an increase in hospital mortality, long-term development of renal failure, and end-stage kidney disease. The observation of the renal microvascular rarefaction can be used to monitor CKD progression [4,5]. Although pathophysiological mechanisms are still under investigation, several studies have shown a loss of microvascular density linked to an acute kidney injury [6-8].

Current imaging techniques for the non-invasive quantification of renal microvascular changes are still lacking [5]. Indeed, magnetic resonance imaging (MRI) [9], computed tomography (CT) [10], and ultrasound (US) [11] have been used to assess changes in renal microcirculation but all these perfusion methods provide indirect quantification without direct access to the microvasculature. Ultrasound has the advantage of safety, non-invasiveness, portability, affordability, and ease of use. Several approaches, such as Doppler imaging and Contrast-Enhanced Ultrasound (CEUS), have been explored in animals and humans [11]. However, none of these techniques offers a sufficiently high spatial resolution to assess microvessels, mainly due to the acoustic diffraction [12].

The concept of Ultrasound Localization Microscopy (ULM) imaging was recently introduced [12] and improves the resolution of the vascular system way beyond the acoustic diffraction limit [13]. ULM is achieved by combining microbubbles, constitutive of ultrasound contrast agents [14], ultrafast ultrasound imaging, [14], and post-processing steps: filtering that extracts signals from microbubbles circulating in the vessels [15], sub-pixel localization of individual microbubbles [16], frame to frame pairing of microbubbles for temporal tracking of their paths in blood vessels and final image reconstruction by the accumulation of microbubbles count. In previous studies, ULM has been successfully tested for in vivo microvessels imaging in rat brains [14], rat kidneys [14], mouse kidneys [4], and in several human organs [17, 18]. However, these studies required research on ultrafast ultrasound scanners which are not common in hospitals. Other studies have been performed with conventional clinical scanners [19], but none in the field of kidney vasculature.

Our objective was to test the hypothesis that the kidney microcirculation sensitivity of ULM on a low frame rate clinical machine could image the micro-vascularization of kidney transplant recipients (KTRs). There was no modification to the imaging system and the post-processing steps were performed directly on the clips recorded by the scanner. Therefore, this technique

will be easy to replicate without having to develop new hardware. In this article, we describe the imaging protocol and post-processing steps needed to perform ULM on any existing setup. Furthermore, we provide a side-by-side comparison of ULM with state-of-the-art Doppler modes. Finally, we investigated the relationship between vessel velocities and their distances to the kidney capsule within the cortex.

METHODS

The French College of Radiology ethics committee approved this study (n° IRB: CRM-2112-218). The work described here has been carried out by The Code of Ethics of the Declaration of Istanbul. All methodologies are detailed in the Supplementary Methods, including subject inclusion, contrast agent injection optimization (Supplementary Figures S1), data acquisition, data optimization, data processing (Supplementary Figures S2), vessel diameter measurements (Supplementary Figures S3, Supplementary Table S1), and kidney capsule segmentation for quantitative speed analysis (Supplementary Figures S4).

In total, the study included 49 KTRs, 35 of whom were used to optimize the method. The results on 7 patients are reported in this article (details in Supplementary Methods).

RESULTS

ULM density and directivity maps

Interlobar vessels, arcuate vessels, cortical radial vessels, and part of the medullary organization are visible on ULM density maps (Figure 1a, 1b). Smaller structures are not clearly detectable by clinical ULM at a low frame rate. ULM directivity maps, i.e. upward flows in red and downward flows in blue, highlighted cortical radial veins and arteries more precisely (Figure 1c, 1d), especially in the upper regions where the vessels are aligned in the axial direction (Figure 1e, 1f). The medullary vasa recta can be seen but are not as clear as the cortical vessels.

Comparison of ULM with Doppler modes

Interlobar vessels, arcuate vessels, and cortical radial vessels are more visible with ULM (Figure 2d) than with other Doppler techniques (Figure 2a-c). In addition, in this same figure, the medullary organization is visible by the ULM density map in patient 1 whereas it is not with other Doppler modes (Figure 2). Five imaged vessel diameters have been estimated for each technique by manual cross-section (Supplementary Figures S3) in 7 patients (Table. 1). The average of the smallest vessel in the 7 patients measured 0.3 ± 0.2 mm for ULM, 0.8 ± 0.3 for Superb Microvascular Imaging (SMI), 1.2 ± 0.4 for Advanced Dynamic Flow (ADF) and 1.3 ± 0.5 for Color Doppler; i.e. 2 to 4 times thinner with ULM than with usual Doppler techniques.

Quantitative speed analysis in the cortex area

ULM speed maps (Figure 3a, 3b) and their further analysis on upper cortex tracks (Figure 3c, 3d) indicate an increase in velocity as the vessels move away from the kidney capsule in two patients (Figure 3c, 3d, Supplementary Figures S4). The averaged velocities of 7 patients who underwent the same capsule segmentation also allow observing this tendency (Figure 3e).

DISCUSSION

In this study, we have shown the feasibility of ULM in kidney transplant recipients using a conventional low frame rate clinical ultrasound scanner. We demonstrated that with very minor adjustments to the examination procedure and simple post-processing tools, we were able to improve the resolution of vascular imaging. We showed that ULM density and directivity maps revealed the different renal structures and that ULM maps reached 2 to 4 times thinner vessel diameter than the conventional high-resolution Doppler modes. Furthermore, we have shown that velocities in cortical regions depend on their distance from the renal capsule: ULM is therefore sensitive enough to detect changes in microvasculature enabling quantitative analysis. These results suggest that ULM could be used in clinical routine to detect microvascular alterations in various kidney diseases [4-8]. In the case of fibrosis or interstitial nephropathy, for example, ULM could be performed instead of pathological analysis by biopsy, thus avoiding risks of bleeding, pain or too small sample size. Changes in kidney microvascularization in addition to morphology can be quantified, as it has already been done in rats [4] and mice [5]: thus, ULM could serve as a new in vivo companion biomarker for the diagnosis of chronic kidney diseases, given that there is no gold standard in imaging yet. Moreover, considering that clinical ultrasound scanners are widely available, such investigation could be replicated on diverse organs without having to develop new equipment.

Nevertheless, several limitations can be identified in this proof-of-concept of clinical ULM in human kidney allograft. First, acquisitions in 35 patients were exploited for optimization leading to a limited number of patients with complete data (details in Supplementary Methods). Besides, the layout of the kidney allografts and the singularity of each patient forced us to carry out segmentations of kidney capsules, upper cortex area (Supplementary Figures S4), and cross-sections by hand (Supplementary Methods, Supplementary Figures S3). In addition, conventional Doppler imaging and ULM are not exactly in the same plane because the probe is hand-held and the examinations are minutes apart. Quantitative estimations are therefore biased and should be taken as indicative.

In addition, since ULM is based on the tracking of microbubbles between images, the maximum velocities observable by ULM are low because of our low frame rate: this confines our sensitivity to large vessels. Ultrafast imaging can improve the estimation of the velocities, but it is not easily accessible in clinics.

Finally, the superficial (heterotopic) position of the renal graft is an advantage for this technique, because the graft is less mobile. ULM could be applied to the native kidney but not without difficulty. The depth of the organ makes it less accessible and more impacted by

breathing: apnea is therefore necessary to be able to perform ULM on the native kidney, which limits the duration of the clips and therefore the richness of the ULM mapping. In obese patients, the depth of the organ due to the thickness of the subcutaneous tissue makes it less accessible. Nevertheless, we still managed to obtain ULM mapping on 2 obese and 3 overweight patients (Supplementary Table S2).

In the future, imaging a native kidney in patients with kidney diseases will be needed to identify the different ULM biomarkers. The ULM's performance could also be improved by using a US probe with a higher frequency to increase the spatial resolution, increasing the signal-to-noise ratio with upgraded signal processing techniques [16], and using a 3D probe [20] that could allow a much faster and more reliable diagnosis.

DISCLOSURE

O.C. and V.H., hold patents in the field of ultrasound localization microscopy (EP4011299A1). O.C. and V.H. are founders and shareholders of the ResolveStroke startup.

Other authors have nothing to declare.

We would also like to declare that the Aplio i800 (Canon MS, Nasu, Japan) ultrasound scanner from which the data was obtained was loaned to the Department of Nephrology and Kidney Transplantation, Necker University Hospital (APHP).

In addition, we want to mention the funding of Bracco at CRIN as a teaching aid.

LIST OF SUPPLEMENTARY MATERIALS

FIGURE TITLES AND LEGENDS

Figure. 1. Ultrasound Localization Microscopy (ULM) density and directivity maps. (a) ULM density map of two renal lobes vasculature in the first patient. “C” is for renal cortex, “M” for medullary organization, “1” for interlobar vessels, “2” for arcuate vessels, “3” for interlobular vessels (cortical radial vessels) and “4” for vasa recta. **(b)** ULM density map of three renal lobes in the second patient. **(c)** ULM directivity map of the first patient. **(d)** ULM directivity map of the second patient. **(e)** and **(f)** Close-up of the two patients ULM directivity maps.

Figure. 2. Smallest imageable vessel diameter measured in Ultrasound Localization Microscopy and in Doppler classical modes in patient 1. (a) Super Microvascular Imaging, **(b)** Color Doppler, **(c)** Advanced Dynamic Flow, **(d)** Ultrasound Localization Microscopy. The white dotted center marks indicate the smallest imageable blood vessel determined by the cross-section diameter measurement on this specific image. (**e**) Statistical differences between all vessels cross sectioned of all 7 patients in each imaging technique. (**f**) Statistical differences between the smallest imageable vessel for each 7 patients in each imaging technique. Student's t test was performed to quantify the differences between vessel cross sections with a 95% confidence level. The significance of the results is as follows: ns = $P > 0.05$, * = $P \leq 0.05$, ** = $P \leq 0.01$, *** = $P \leq 0.001$, **** = $P \leq 0.0001$.

Figure. 3. ULM speed maps quantitative analysis. (a) ULM speed maps of the first patient. ULM density map has been encoded with the velocity of each track. **(b)** ULM speed maps of the second patient with same encoding. **(c)** ULM tracks only in the cortex with kidney capsule area indicated in yellow line in patient 1. **(d)** ULM tracks only in the cortex with kidney capsule area indicated in yellow line in patient 2. **(e)** Distance to the capsule as a function of the mean speed in 7 patients. The x-axis corresponds to the mean velocity values of all tracks present in the cortex area at a certain distance of the capsule. White dot indicates the median in all 7 patients, and color dots indicate the mean tracks velocity of each patient at this capsule distance.

REFERENCES

1. Carney EF. The impact of chronic kidney disease on global health. *Nat Rev Nephrol*. 2020;16(5):251-251. doi:10.1038/s41581-020-0268-7

2. Chawla LS, Eggers PW, Star RA, Kimmel PL. Acute Kidney Injury and Chronic Kidney Disease as Interconnected Syndromes. *N Engl J Med*. 2014;371(1):58-66. doi:10.1056/NEJMra1214243

3. Leung KCW, Tonelli M, James MT. Chronic kidney disease following acute kidney injury—risk and outcomes. *Nat Rev Nephrol*. 2013;9(2):77-85. doi:10.1038/nrneph.2012.280

4. Chen Q, Yu J, Rush BM, et al. Ultrasound super-resolution imaging provides a noninvasive assessment of renal microvasculature changes during mouse acute kidney injury. *Kidney Int.* 2020;98(2):355-365. doi: 10.1016/j.kint.2020.02.011

5. Li S, Wang F, Sun D. The renal microcirculation in chronic kidney disease: novel diagnostic methods and therapeutic perspectives. *Cell Biosci*. 2021;11(1):90. doi:10.1186/s13578-021-00606-4

6. Basile D, Yoder M. Renal Endothelial Dysfunction in Acute Kidney Ischemia Reperfusion Injury. *Cardiovasc Hematol Disord-Drug Targets*. 2014;14(1):3-14. doi:10.2174/1871529X1401140724093505

7. Hörbelt M, Lee SY, Mang HE, et al. Acute and chronic microvascular alterations in a mouse model of ischemic acute kidney injury. *Am J Physiol-Ren Physiol*. 2007;293(3):F688-F695. doi:10.1152/ajprenal.00452.2006

8. Steegh FMEG, Gelens MACJ, Nieman FHM, et al. Early Loss of Peritubular Capillaries after Kidney Transplantation. *J Am Soc Nephrol*. 2011;22(6):1024-1029. doi:10.1681/ASN.2010050531

9. Prowle JR, Molan MP, Hornsey E, Bellomo R. Measurement of renal blood flow by phase-contrast magnetic resonance imaging during septic acute kidney injury: A pilot investigation. *Crit Care Med*. 2012;40(6):1768-1776. doi:10.1097/CCM.0b013e318246bd85

10. Ehling J, Bábíčková J, Gremse F, et al. Quantitative Micro-Computed Tomography Imaging of Vascular Dysfunction in Progressive Kidney Diseases. *J Am Soc Nephrol*. 2016;27(2):520-532. doi:10.1681/ASN.2015020204

11. Cao W, Cui S, Yang L, et al. Contrast-Enhanced Ultrasound for Assessing Renal Perfusion Impairment and Predicting Acute Kidney Injury to Chronic Kidney Disease Progression. *Antioxid Redox Signal*. 2017;27(17):1397-1411. doi:10.1089/ars.2017.7006

12. Couture O, Hingot V, Heiles B, et al. Ultrasound Localization Microscopy and Super-Resolution: A State of the Art. *IEEE Trans Ultrason Ferroelectr Freq Control.* 2018;65(8):1304-1320. doi:10.1109/TUFFC.2018.2850811

13. Desailly Y, Pierre J, Couture O, Tanter M. Resolution limits of ultrafast ultrasound localization microscopy. *Phys Med Biol.* 2015;60(22):8723-8740. doi:10.1088/0031-9155/60/22/8723

14. Couture O, Bannouf S, Montaldo G, et al. Ultrafast Imaging of Ultrasound Contrast Agents. *Ultrasound Med Biol*. 2009;35(11):1908-1916. doi: 10.1016/j.ultrasmedbio.2009.05.020

15. Desailly Y, Tissier AM, Correas JM, et al. Contrast enhanced ultrasound by real-time spatiotemporal filtering of ultrafast images. *Phys Med Biol.* 2017;62(1):31-42. doi:10.1088/1361-6560/62/1/31

16. Heiles B, Chavignon, A, Hingot V, et al. Performance benchmarking of microbubble-localization algorithms for ultrasound localization microscopy, *Nature Biomedical Engineering*, 2022, (doi.org/10.1038/s41551-021-00824-8).

17. Huang C, Zhang W, Gong P, et al. Super-resolution ultrasound localization microscopy based on a high frame-rate clinical ultrasound scanner: an in-human feasibility study. *Phys Med Biol.* Published online March 16, 2021. doi:10.1088/1361-6560/abef45

18. Demené C, Robin J, Dizeux A, et al. Transcranial ultrafast ultrasound localization microscopy of brain vasculature in patients. *Nat Biomed Eng*. 2021;5(3):219-228. doi:10.1038/s41551-021-00697-x

19. Dencks S, Piepenbrock M, Opacic T, et al. Clinical pilot application of super-resolution US imaging in breast cancer. *IEEE Trans Ultrason Ferroelectr Freq Control.* 2018;66(3):517-526.

20. Chavignon A, Heiles B, Hingot V, et al. 3D Transcranial Ultrasound Localization Microscopy in the Rat Brain with a Multiplexed Matrix Probe. *IEEE Trans Biomed Eng*. Published online 2022:1-1. doi:10.1109/TBME.2021.3137265[2]

ACKNOWLEDGEMENTS

We thank all the staff of the Necker hospital for the good progress of the acquisitions. This study was funded by the European Research Council under the European Union Horizon H2020 program (ERC Consolidator grant agreement No 772786-ResolveStroke).

FIGURES

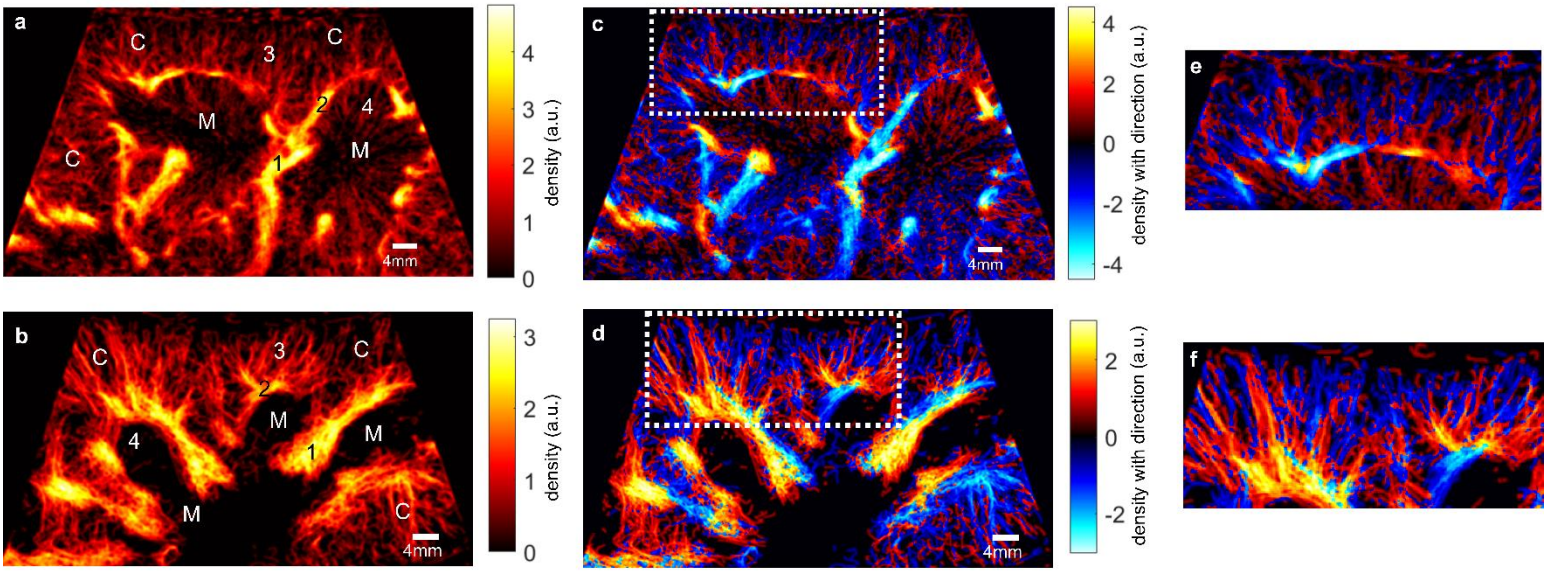

Figure. 1. Ultrasound Localization Microscopy (ULM) density and directivity maps. (**a**) ULM density map of two renal lobes vasculature in the first patient. "C" is for renal cortex, "M" for medullary organization, "1" for interlobar vessels, "2" for arcuate vessels, "3" for interlobular vessels (cortical radial vessels) and "4" for vasa recta. (**b**) ULM density map of three renal lobes in the second patient. (**c**) ULM directivity map of the first patient. (**d**) ULM directivity map of the second patient. (**e**) and (**f**) Close-up of the two patients ULM directivity maps.

241

242

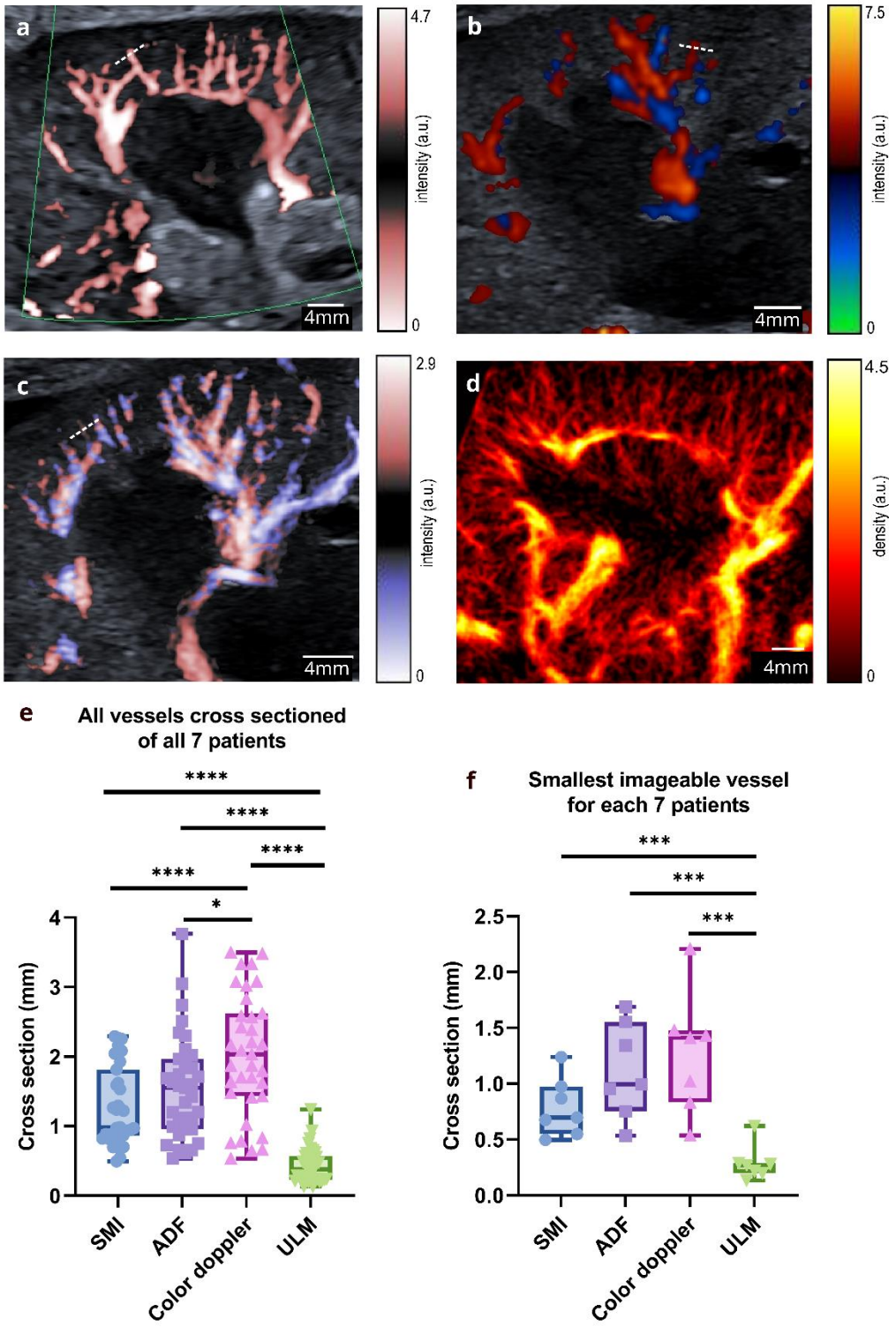

Figure. 2. Smallest imageable vessel diameter measured in Ultrasound Localization Microscopy and in Doppler classical modes in patient 1. (**a**) Super Microvascular Imaging, (**b**) Color Doppler, (**c**) Advanced Dynamic Flow, (**d**) Ultrasound Localization Microscopy. The white dotted center marks indicate the smallest imageable blood vessel determined by the cross-section diameter measurement on this specific image. (**e**) Statistical differences between all vessels cross sectioned of all 7 patients in each imaging technique. (**f**) Statistical differences between the smallest imageable vessel for each 7 patients in each imaging technique. Student's t test was performed to quantify the differences between vessel cross sections with a 95% confidence level. The significance of the results is as follows: ns = $P > 0.05$, * = $P \leq 0.05$, ** = $P \leq 0.01$, *** = $P \leq 0.001$, **** = $P \leq 0.0001$.

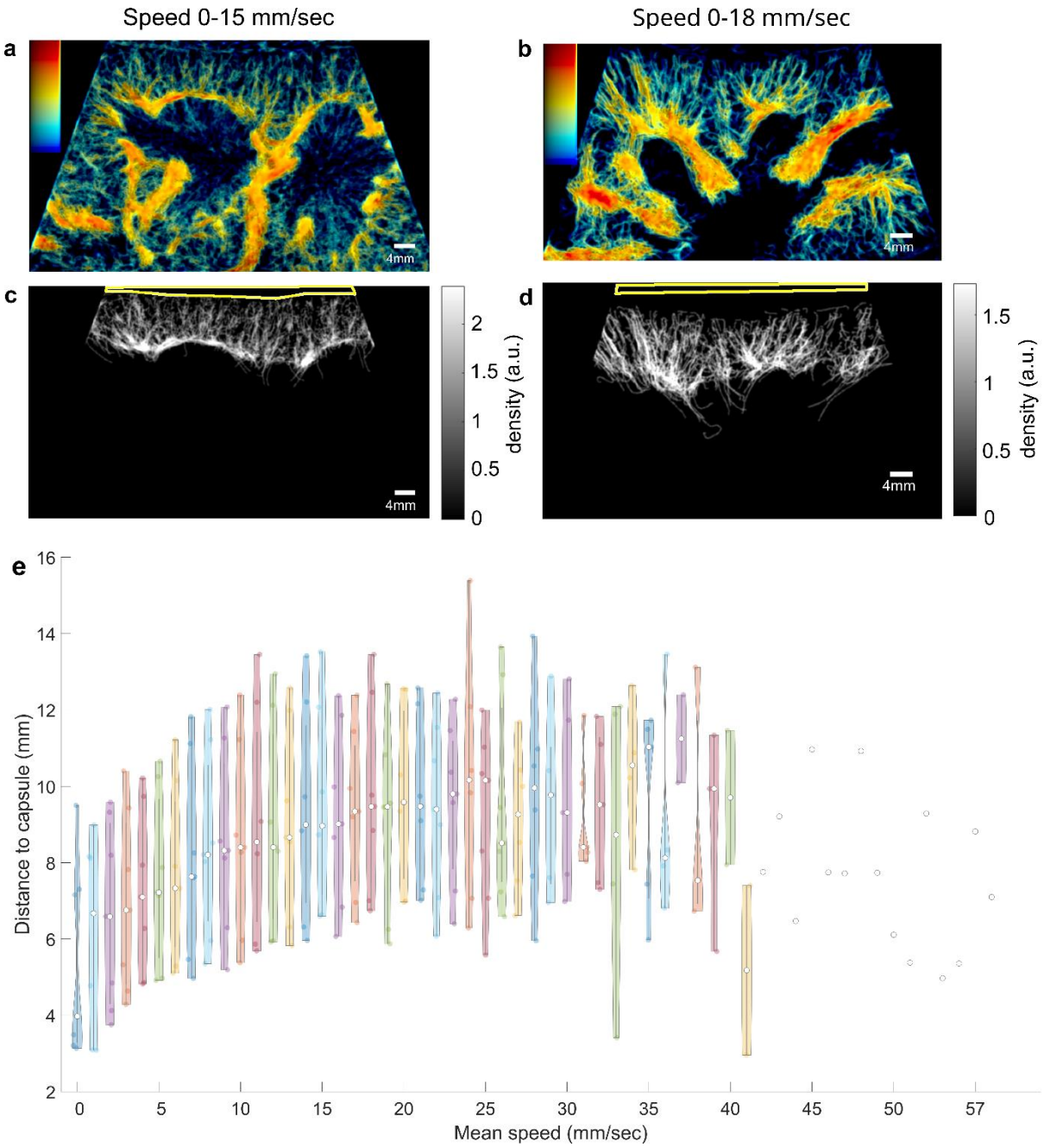

Figure. 3. ULM speed maps quantitative analysis. (**a**) ULM speed maps of the first patient. ULM density map has been encoded with the velocity of each track. (**b**) ULM speed maps of the second patient with same encoding. (**c**) ULM tracks only in the cortex with kidney capsule area indicated in yellow line in patient 1. (**d**) ULM tracks only in the cortex with kidney capsule area indicated in yellow line in patient 2. (**e**) Distance to the capsule as a function of the mean speed in 7 patients. The x-axis corresponds to the mean velocity values of all tracks present in the cortex area at a certain distance of the capsule. White dot indicates the median in all 7 patients, and color dots indicate the mean tracks velocity of each patient at this capsule distance.

243

244 **TABLE**

Imaging technique	Mean (± SD) of the smallest imageable vessel diameter among the 7 patients (mm)	Mean (± SD) of the 7 patients' vessel diameter (mm)
ULM*	0.3 ± 0.2	0.4 ± 0.2
SMI** + contrast agent	0.8 ± 0.3	1.3 ± 0.6
ADF***	1.2 ± 0.4	1.5 ± 0.7
Color Doppler	1.3 ± 0.5	2.0 ± 0.9

Table. 1. **Cross-section measurements for each imaging technique in 5 vessels per patient on 7 patients.** We noted the mean (± standard deviation) of the smallest imageable vessel diameter among the 5 vessels of each 7 patients and the mean (± standard deviation) of the 5 vessels of every 7 patients' diameter.
*Ultrasound Localization Microscopy (ULM), **Superb Microvascular Imaging (SMI), ***Advanced Dynamic Flow (ADF).

245

SUPPLEMENTARY MATERIAL

Supplementary Methods

From February to August 2020, 49 kidney transplant recipients older than 18 years were included. Patients were those who were previously referred for ultrasound examination in our adult radiology department at Necker University Hospital. In clinical routine, these subjects receive several postoperative ultrasounds: on day 1, then on month 3, on month 12, and annually. They also receive ultrasound scans in case of graft dysfunction to explore a surgical or medical complication. The examination includes B-mode, classical Dopplers (Color Doppler, Superb Microvascular Imaging, and Advanced Dynamic Flow), and pulsed Doppler acquisitions. An ultrasound acquisition with Sonovue® microbubbles injection (Bracco) is also performed to explore hypo- or avascular areas and necrosis: thus, no additional injection was necessary for this study and we used the same type of acquisition to perform the ULM. In addition, to avoid motion artifacts in the acquisitions, patients were supine and breathing slowly.

We started to optimize the CEUS mode embedded in the clinical scanner on the first 15 patients to have satisfactory ULM images. To perform ULM, we used an Aplio i800 (Canon MS, Nasu, Japan) and an i8CX1 convex abdominal probe (3 MHz). Probes used to perform conventional Doppler techniques were either i8CX1 (3MHz) or i11LX3 (7MHz). The dynamic range and gain were adapted to the ultrasound machine, which allowed better discrimination of microbubbles and facilitated their localization. Because of the superficial position of the renal graft in the iliac fossa, we were able to reduce the imaging depth to explore between 4 and 10 cm, resulting in a maximum clip time of 1 to 3 minutes. In this way, we could increase the frame rate (between 14 and 64Hz). Data were collected in DICOM format and all dynamic clips were stored anonymously on a hard disk. From 2 to 4 clips were stored per patient resulting in a total of 142 clips for the 49 patients. All data analyses were performed at the Biomedical Imaging Laboratory by members of the PPM (Physiology Pathology of the Microcirculation) team, specialist in ULM for over 5 years.

After optimization of the probe's positioning on 5 patients, we searched for time-window with the optimal number of microbubbles on 15 patients. The injection of a bolus of 1.2 mL of microbubbles, followed by an injection of 10 ccs of saline, was repeated twice, as in the clinical routine. The optimal number of microbubbles, i.e. to have isolated ones, was reached during

the late venous phase, i.e. on average between 45 and 192 seconds after injection. The difference in microbubbles concentration between a too-early phase (too many microbubbles), an optimum phase (many distinct microbubbles), and a delayed phase (disappearing microbubbles) was observed in CEUS acquisitions (Supplementary Figures S1). We used a low mechanical index (=0.07) to exploit the non-linear properties of microbubbles [S1] by limiting their destruction. The examination duration then depends almost exclusively on the natural lifetime of the microbubbles in the blood compartment.

In short, from the 49 included KTRs, 35 were used for the optimization of CEUS mode, probe's positioning, and microbubbles optimal number targeting. The remaining 14 were used to perform ULM, and among them, 7 were excluded because of respiratory movements: results on the remaining 7 are presented in this study.

To do ULM images, clips were divided into blocks of 200 frames each: a clip of 173 seconds at 22 Hz corresponding to 3812 consecutive frames was thus divided into 20 blocks. ULM was achieved with classical steps on each block: filtering, localization of microbubbles, tracking, and track accumulation. Filtering was already done by the CEUS mode embedded in the ultrasound system (Supplementary Figures S2a): bandpass filters with cutoff frequencies from 0.5 to 8.5Hz have been added to enhance the moving microbubbles. Localization has been realized thanks to a 2-D Gaussian filter with a standard deviation of 1 pixel (i.e. from 0.07 to 0.17mm) and targeting of the regional maximums (Supplementary Figures S2b). Tracking was performed with the Hungarian algorithm method [S2] using a maximum distance between the microbubbles of 1 to 2.8mm and a minimum track duration varying from 0.08 to 0.4 seconds (Supplementary Figures S2c). Finally, tracks accumulation of the 8 to 35 blocks, allowed us to obtain a vascular density map of the kidney (Supplementary Figures S2d).

We keep the same pixel size for ULM maps as the original grid (from 0.07 to 0.17mm). We measured five vessels' diameters in Doppler modes and ULM with the cross-section technique [S3, S4] (Supplementary Figures S3) in every 7 patients: we thus have an estimation of the mean of these thirty-five vessels' diameters, their standard deviation, and an estimation of the average of the 7 smallest vessels for each technique. The intensity of the red component was used to estimate diameter on ADF, SMI, and color Doppler (color of segmented vessels).

It is important to specify that these measurements are not resolution measurements but measurements of the vessels' diameters, which can give us an idea of the resolution achieved by each of the ultrasound techniques. Pixel size of each ultrasound techniques, also called spatial resolution, have been described in Supplementary Table S1.

Velocity encoding was performed and overlaid on the density map. Directions were encoded in red when tracks go towards the probe, and in blue when they go away from it. To perform a quantitative ULM analysis, we manually segmented the kidney capsule and upper cortex area to investigate a potential correlation between vessel velocity and its distance to the capsule (Supplementary Figures S4). This analysis was performed only on tracks present in the upper cortex for two reasons: the lower kidney capsule was not visible on acquisitions, and to avoid aliasing bias present in the bigger vessel by ULM. Indeed, max speed detected by ULM varies from 2cm/sec to 6cm/sec whereas biggest kidney vessels speed is normally around 100cm/sec [S5].

All image processing was made with MATLAB (Mathworks).

Statistical analyses were performed with Graphpad Prism 9 software. Student's t test was performed to quantify the differences between vessel cross sections with a 95% confidence level. The significance of the results is as follows: ns = $P > 0.05$, * = $P \leq 0.05$, ** = $P \leq 0.01$, *** = $P \leq 0.001$, **** = $P \leq 0.0001$.

SRQR reporting guidelines were applied [S6].

Supplementary Figures

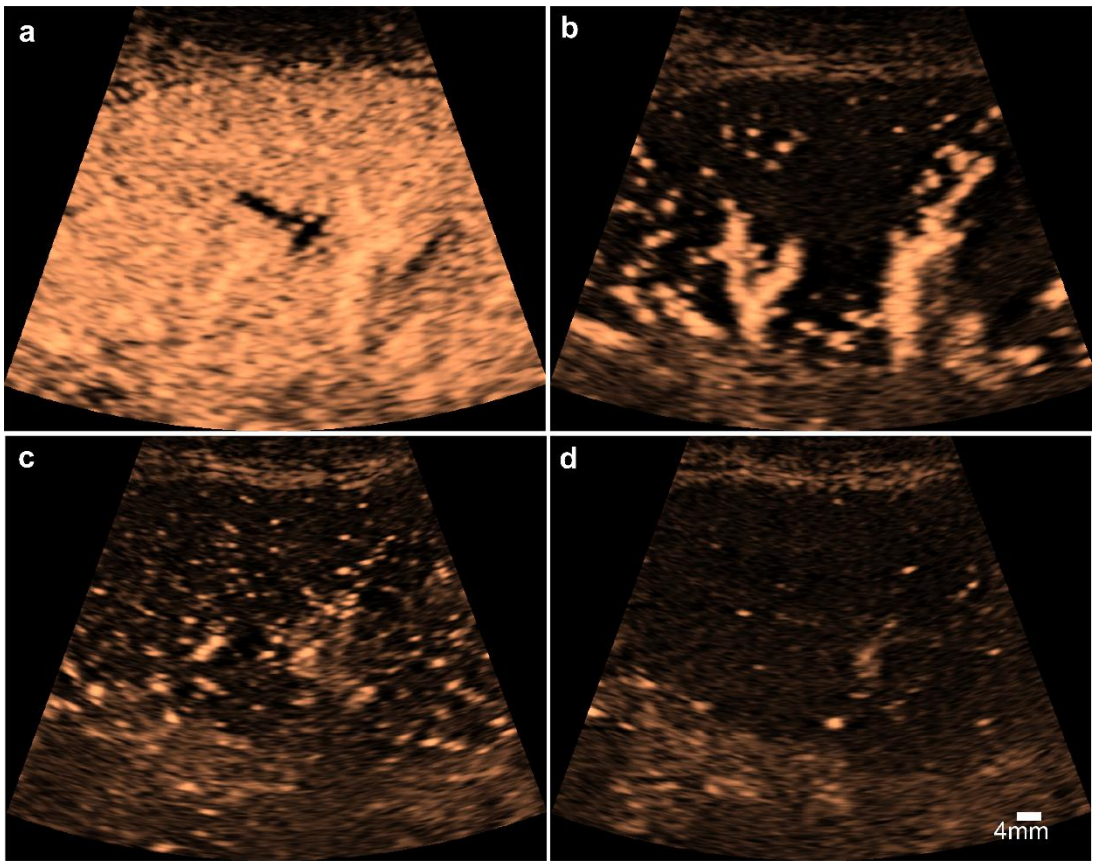

Supplementary Figure. S1. Difference in microbubbles concentration in patient 1. (**a**) Contrast Enhanced Ultrasound acquisitions in clinical practice. (**b**) Microbubbles early arrival. (**c**) Late venous phase (optimal phase). (**d**) Very delayed phase. The colormap comes from the ultrasound scanner without specification (arbitrary unit). The scale bar is the same as in d for all 4 images.

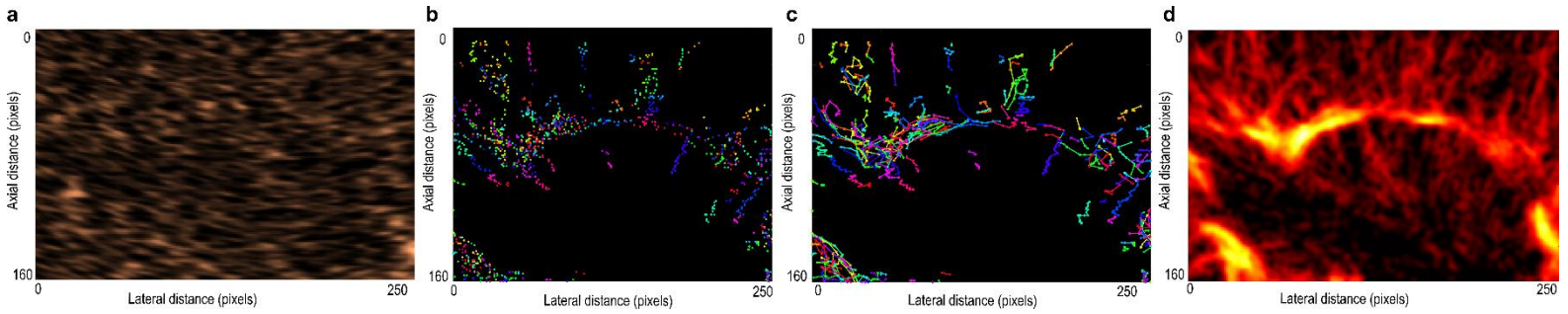

Supplementary Figure.S2. Framework of ULM image formation in zoomed patient 1. (**a**) Contrast Enhanced Ultrasound (CEUS) acquisition with a clutter filter integrated in the clinical echograph. The color map comes from the ultrasound scanner without specification (arbitrary unit). (**b**) Localization of microbubbles thanks to a 2D gaussian filter in one bloc (arbitrary colors). (**c**) Tracking thanks to Hungarian algorithm in the same bloc (arbitrary colors). (**d**) ULM density map resulting from the accumulation of twenty blocs (density colormap from 0 to 4.5 in arbitrary units).

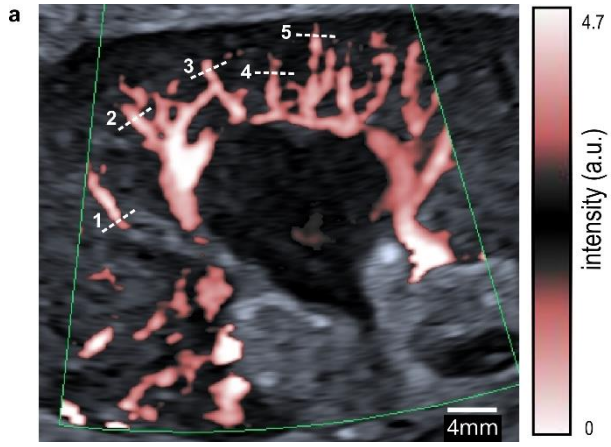

Supplementary Figure.S3. Example of cross-section measurement in Superb Microvascular Imaging (SMI), with contrast agent, acquisition in patient 1. (**a**) SMI, with contrast agent, image with five cross-sectioned vessels indicated with dotted white lines. The color map comes from the ultrasound scanner without specification (arbitrary unit). (**b**) Diameter measured as the width at half the maximum intensity (of the red component), in the third manually cross-sectioned vessel. Red arrow indicates the width at half the maximum intensity.

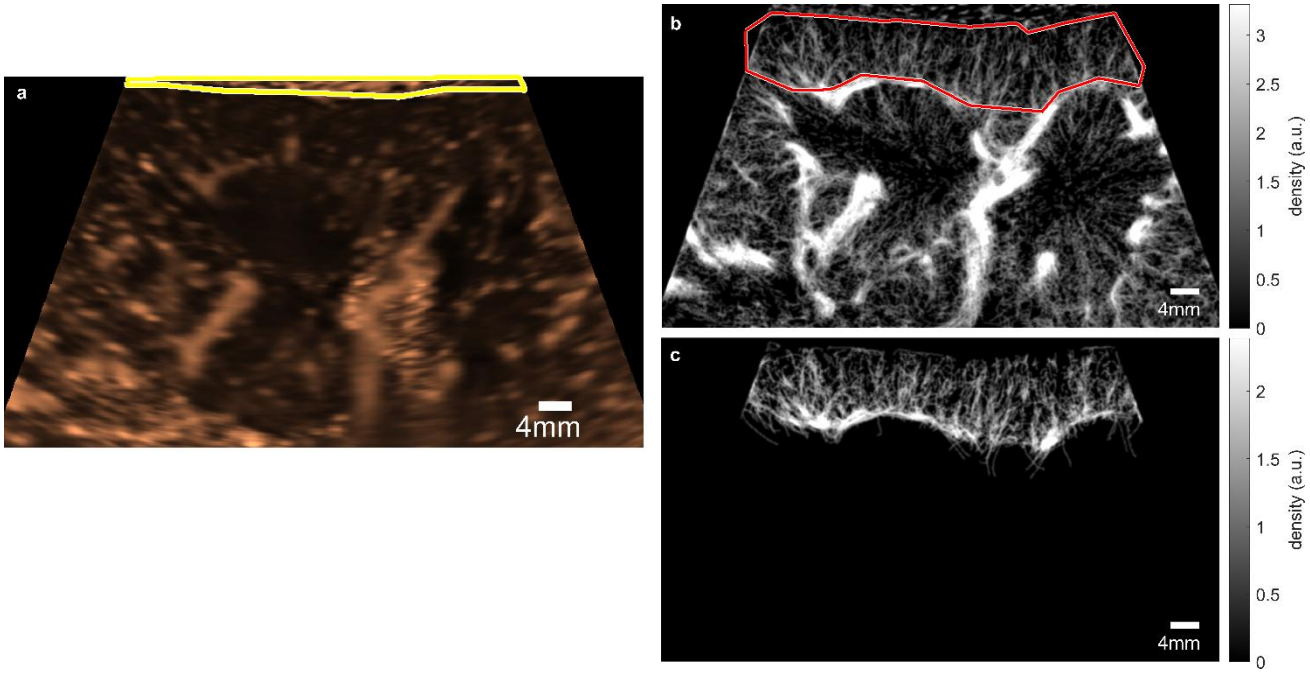

Supplementary Figure.S4. Kidney capsule and upper cortex manual segmentation on patient 1. (**a**) Capsule segmentation made on temporal mean of the first block of CEUS acquisition in patient 1. Kidney capsule is indicated with a yellow line. The color map comes from the ultrasound scanner without specification (arbitrary unit). (**b**) Upper cortex segmentation made on ULM density map. Cortex mask is drawn with a red line. (**c**) Resulting cortex tracks from the upper cortex segmentation. If at least one point of a track was present in the upper cortex mask, track was preserved.

Supplementary Tables

Patients n°	Pixel resolution (mm)			
	CEUS	ADF	SMI	Color Doppler
1	0.12	0.07	0.10	0.07
2	0.07	0.15	0.15	0.18
4	0.12	0.15	0.07	0.18
10	0.14	0.08	0.13	0.15
11	0.17	0.18	0.17	0.17
13	0.15	0.18	0.13	0.17
19	0.10	0.13	0.15	0.13

Supplementary Table S1. Pixel resolution of each ultrasound modes in each patient.

Patient number	Etiology of initial renal failure	Sonovue Dose (mL)	Time frame of the transplantation	Dilation of the pyelo-caliceal cavities	SRT (ms)	RI interlobar arteries	Nb of grefon veins	Nb of grefon arteries	Creatinin (µmol/L)	Graft depth (mm)	BMI (kg/m²)	Age (y)	Sex
1	Cystinosis	1.2	11 days	No	<200	0.72 - 0.82	1	1	105	9	31	33	F
2	Valve of the posterior urethra	1.2	12 hours	No	<200	0.41 - 0.52	1	1	180	15	24	19	M
3	TSB + ADPKD	1.2	3 days	No	<200	0.82 - 0.89	1	2	203	36	25	36	F
4	MPGN	1.2	17 days	No	<200	0.62 - 0.65	1	1	130	24	21	19	M
5	Diabetic nephropathy	1.2	24 hours	No	<200	0.76 - 0.92	1	2	111	27	28	55	M
6	Nephropathy indeterminate	1.2	6 months 3 days	No	<200	0.67 - 0.72	1	2	200	14	32	28	M
7	Berger's disease	1.2	10.5 years	No	<200	0.75 - 0.85	1	1	380	15	29	68	M

Supplementary Table S2. Patient characteristics.

TSB: Tuberous sclerosis of Bourneville; ADPKA: Autosomal Dominant Polycystic Kidney Disease; IR: Resistance Index; SRT: Systolic Rise Time; MPGN: Membranoproliferative glomerulonephritis.

Supplementary References

S1. Brown J, Christensen-Jeffries K, Harput S, et al. Investigation of Microbubble Detection Methods for Super-Resolution Imaging of Microvasculature. *IEEE Trans Ultrason Ferroelectr Freq Control*. 2019;66(4):676-691. doi:10.1109/TUFFC.2019.2894755

S2. Tinevez JY, Perry N, Schindelin J, et al. TrackMate: An open and extensible platform for single-particle tracking. *Methods*. 2017;115:80-90. doi:10.1016/j.ymeth.2016.09.016

S3. Errico C, Pierre J, Pezet S, et al. Ultrafast ultrasound localization microscopy for deep super-resolution vascular imaging. *Nature*. 2015;527(7579):499-502. doi:10.1038/nature16066

S4. Hingot V, Errico C, Heiles B, et al. Microvascular flow dictates the compromise between spatial resolution and acquisition time in Ultrasound Localization Microscopy. *Sci Rep*. 2019;9(1):2456. doi:10.1038/s41598-018-38349-x

S5. Pellerito J, Polak J. Introduction to Vascular Ultrasonography. *Elsevier Health* Sciences; 2019.

S6. O'Brien BC, Harris IB, Beckman TJ, et al. Standards for reporting qualitative research: a synthesis of recommendations. *Acad Med.* 2014;89(9):1245-1251.